Inorganic Chemistry

Forum Article

pubs.acs.org/IC

Taming Lanthanide-Centered Upconversion at the Molecular Level

Yan Suffren,[†] Bahman Golesorkhi,[‡] Davood Zare,[‡] Laure Guénée,[§] Homayoun Nozary,[‡] Svetlana V. Eliseeva,[⊥] Stéphane Petoud,[‡,⊥] Andreas Hauser,[†] and Claude Piguet*[,‡]

[†]Department of Physical Chemistry, [§]Laboratory of Crystallography, and [‡]Department of Inorganic and Analytical Chemistry, University of Geneva, 30 quai E. Ansermet, CH-1211 Geneva 4, Switzerland

[⊥]Centre de Biophysique Moléculaire, CNRS UPR 4301, Rue Charles Sadron, F-45071 Orléans Cedex 2, France

Supporting Information

ABSTRACT: Considered at the beginning of the 21th century as being incompatible with the presence of closely bound high-energy oscillators, lanthanide-centered superexcitation, which is the raising of an already excited electron to an even higher level by excited-state energy absorption, is therefore a very active topic strictly limited to the statistical doping of low-phonon bulk solids and nanoparticles. We show here that molecular lanthanide-containing coordination complexes may be judiciously tuned to overcome these limitations and to induce near-infrared (NIR)-to-visible (VIS)-light upconversion via the successive absorption of two low-energy photons using linear-optical responses. Whereas single-ion-centered excited-state absorption mechanisms remain difficult to implement in lanthanide complexes, the skillful design of intramolecular intermetallic energy-transfer processes operating in multimetallic architectures is at the origin of the recent programming of erbium-centered molecular upconversion.

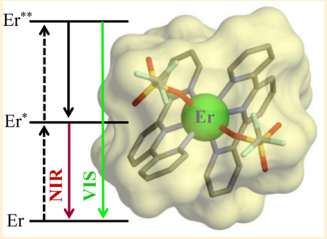

OPTICAL ANTI-STOKES PROCESSES AT THE TURN OF THE 21ST CENTURY: A DRIVE FOR TECHNOLOGICAL APPLICATIONS

Although the Kerr effect, which states that the refractive index of a material varies both linearly and quadratically with the applied electric field, was discovered at the end of the 19th century,[1] the possibility of combining two low-energy photons in order to obtain one photon of higher energy as a result of the nonlinear dependence of the refractive index on the oscillating electric field of an incident excitation radiation was theoretically predicted only in 1931.[2] Its experimental illustration for second harmonic generation (SHG; Figure 1a)[3] and for two-photon excitation fluorescence (TPEF; Figure 1b)[4] was delayed until the first ruby laser became available in 1960.[5] Because of the very small nonlinear-optical (NLO) two-photon absorption cross sections, despite the recurrent attempts to optimize NLO responses in sophisticated polar push−pull π−aromatic molecules,[6] these phenomena require intense and coherent laser irradiation, typically in the range of MW cm^{-2} to provide detectable emission.[7] Application-oriented developments of NLO at the molecular level are therefore restricted to systems tolerating high-intensity irradiation, such as, for instance, in photobiology using optimized organic chromophores[8] or in two-photon-excited microscopy experiments exploiting luminescent lanthanide complexes.[9] The early 1960s also saw the discovery of sequential absorptions, this time with the exclusive resort to linear optics, of two infrared (IR) excitation photons to reach an excited state, the emission energy of which exceeds the incident radiation by 10−100 times kT.[10] This phenomenon, often referred to as superexcitation or excited-state absorption (ESA), is now grouped under the general terminology of upconversion (Figure 1c).[11] The existence of real intermediate excited states in the upconversion mechanism, rather than virtual states pertinent for NLO, increases the efficiency of the anti-Stokes emission by up to 8 orders of magnitude. This improvement can be further extended by 2 orders of magnitude when energy-transfer processes replace the successive excitations in APTE processes (addition de photons par transferts d'énergie),[12] later termed ETU for energy-transfer upconversion (Figure 1d).[13]

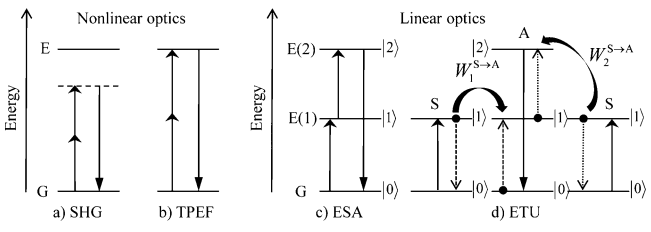

Figure 1. Energy-transfer schemes for selected two-photon processes (G = ground state; E = excited state): (a) nonresonant SHG; (b) resonant TPEF; (c) ESA; (d) sequential ETU. A = activator, S = sensitizer, and $W^{S\to A}$ = intermolecular S → A energy-transfer probabilities.

Beyond some residual questions regarding fundamental scientific challenges with the ultimate goal to push back limits of upconversion in terms of both mechanisms and rationalization,[14] the major part of research activity has been focused on the systematic and empirical optimization of the efficiency of lanthanide-centered upconversion implemented in inorganic

Special Issue: New Trends and Applications for Lanthanides

Received: March 23, 2016
Published: May 20, 2016

DOI: 10.1021/acs.inorgchem.6b00700
Inorg. Chem. 2016, 55, 9964−9972

oxides, fluorides, garnets, or mixed oxides.[11,15] Beyond some niche applications in wave guides,[16] security inks,[17] lasers, and display devices,[18] the most attractive and potentially profitable developments of these solid-state upconverters concern the reduction in spectral mismatch for solar cell technology[11c,19] and the design of bioprobes,[20] which could be excited in the NIR, where biological tissues are globally transparent.[21] To the best of our knowledge, the highest intrinsic upconversion quantum yields (i.e., number of emitted upconverted photons compared with the number of absorbed photons) reported to date for lanthanide-centered upconversion occurring in bulk singly doped materials are 12(1)% for Gd_2O_2S:10% Er^{3+} and 8.9(7)% for β-$NaYF_4$:25% Er^{3+},[22] while a value of 4% seems pertinent for the multiply doped fluoride β-$NaYF_4$:18% Yb^{3+}-2% Er^{3+}.[23] Attempts to reduce the size of the material to reach nanometric scales compatible with their incorporation into biological organisms drastically increase the surface-to-volume ratio, and the upconversion efficiency drops as the surface states quench the emission signal.[15,24] The latter multiply doped material β-$NaYF_4$:18% Yb^{3+}-2% Er^{3+} (4% quantum yield estimated as a bulk solid), manufactured as 30-nm-diameter nanoparticles, displays quantum yields of around 0.1%, which can be improved to 0.3% with the deposit of a passivating shell.[25] Let us stress here that, even if the intrinsic upconversion quantum yield is acceptable, the external upconversion quantum efficiency, that is, the ratio of the number of emitted upconverted photons over the total number of incident photons, is drastically limited by the small absorption cross sections of f−f transitions in trivalent lanthanides (on the order of $\sigma \approx 10^{-20}$ cm^2).[26] In this context, the coupling of nanoparticles to a surface plasmon has been explored to enhance the local electromagnetic fields, which results in increased absorption cross sections and faster radiative decay rates.[27] Nevertheless, the resulting improved upconversion efficiencies are still not sufficient for technological applications aimed at converting the NIR part of the solar light into green emission for its absorption by dye-sensitized or crystalline silica solar cells (the power density of the terrestrial solar irradiance is approximately 0.1 W cm^{-2}).[19] Because long-lived intermediate excited states that have characteristic lifetimes within the millisecond range are required for the successful collection of a second excitation process in lanthanide-centered upconversion, their implementation at the molecular level in open-shell lanthanide coordination complexes possessing high-energy vibrations/phonons and short excited-state lifetimes is not easily conceivable.[28] Alternatively, closed-shell polyaromatic molecules made of light atoms with negligible spin−orbit coupling constants possess long-lived intermediate triplet excited states, which are compatible with energy storage on two molecular partners following an initial irradiation (Figure 2).[29] This sensitized noncoherent upconversion based on triplet−triplet annihilation (TTA) of a pair of organic molecules, first illustrated in the early 1960s,[30] is indeed initiated by a spin-allowed $\pi \rightarrow \pi^*$ transition located on the sensitizer, S, which is responsible for a highly efficient light-harvesting process because the involved linear extinction coefficients can reach $\varepsilon \approx 10^5$ M^{-1} cm^{-1} ($\sigma \approx 4 \times 10^{-16}$ cm^2).[31] Subsequent intersystem crossing establishes a long-lived triplet excited state $^3S^*$, which undergoes intermolecular $^3S^*/^1A \rightarrow {}^1S/{}^3A^*$ Dexter-type triplet−triplet energy transfer with a neighboring acceptor, A. The $^3A^*$ triplet state is sufficiently long-lived to diffuse and collide with a second identical partner. TTA then produces a mixture of singlet, triplet, and quintet excited-state dimers, in which the $^3A^* + {}^3A^* \rightarrow {}^1A^* + {}^1A$ pathway leads to the targeted high-energy singlet excited state located on the acceptor. Relaxation of the $^1A^*$ state to the ground state is finally accompanied by the emission of a photon of higher energy than those involved in the excitation process, that is, an upconverted emission (Figure 2).[32]

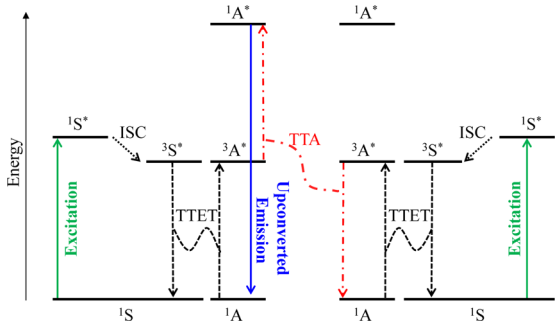

Figure 2. Qualitative Jablonski diagram illustrating the sensitized TTA upconversion process operating in a S/A mixture. Colored solid arrows indicate transitions in which a photon is involved, while black dashed arrows indicate radiationless processes (ISC = intersystem crossing and TTET = triplet−triplet energy transfer). The red dash-dotted arrows stand for TTA.

The calculated excitation rate constants $k_{exc} \sim 10$ s^{-1} operating in organic aromatic sensitizers,[31] combined with remarkable 16−26% intrinsic upconversion quantum yields observed in 9,10-diphenylanthracene/platinum octaethylporphyrin organic pairs,[32c] provide exploitable green-to-blue molecular upconverters operating under standard noncoherent AM1.5G solar irradiation.[32] However, the requirements for the diffusion and collision of two triplet excited-state acceptors for TTA limit this methodology to intermolecular processes occurring in solution, rubbery polymeric materials, or solid matrixes, which ensure the efficient diffusion of molecules and/or molecular excitons under anaerobic conditions (dioxygen can easily quench triplet excited states).[31,32] Finally, photobleaching remains a major issue with organic dyes, which is difficult to reconcile with long-term operation periods. We therefore foresee that lanthanide-doped bulk materials are the most promising upconverters for potential applications in solar cell technology, whereas the interest for upconverting nanoparticles will decrease because of their reduced quantum yields. On the other hand, the requirements for bioanalytical and biomedical applications in terms of size are better fitted by upconverting nanoparticles, but the difficulties linked to their synthetic reproducibility and to their uncontrolled degradation in living organisms are severe limitations. The latter drawbacks could be overcome by molecular lanthanide complexes if large-enough quantum yields could be achieved for these high-energy phonon materials.

ONE-CENTER SUPEREXCITATION IN MOLECULAR COMPLEXES: THE ESA MECHANISM

A one-center superexcitation of lanthanide activator A in a bulk solid or in a coordination complex (Figure 1c) can be modeled with the kinetic scheme depicted in Figure 3a, in which each first-order rate constant corresponds to either an intramolecular excitation $k_A^{exc(i\rightarrow j)}$ or relaxation processes $k_A^{i\rightarrow j}$.[35] The set of first-order differential equations required for estimating the time-dependent changes in the normalized population densities of

DOI: 10.1021/acs.inorgchem.6b00700
Inorg. Chem. 2016, 55, 9964−9972

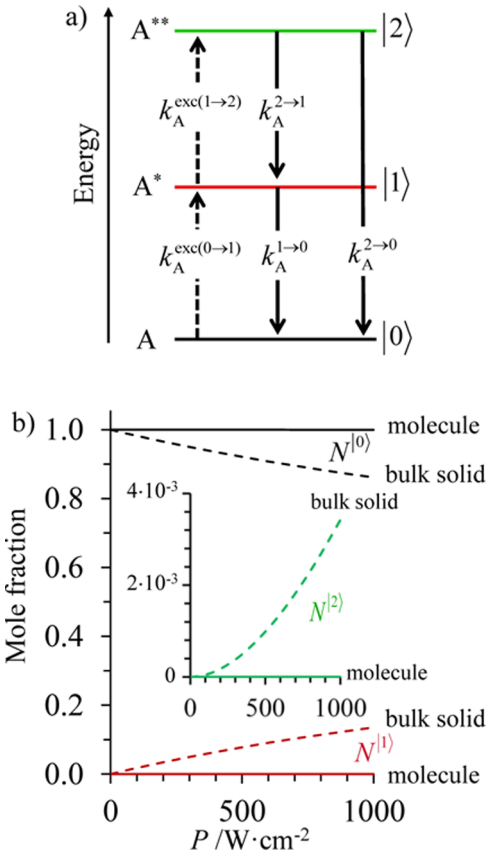

Figure 3. (a) Kinetic scheme depicting the modeling of the single- ion ESA process occurring upon off-resonance irradiation into the activator-centered absorption band. $k_A^{1\to0}$ stands for the global decay rate constant of the first A* excited state, and $k_A^{2\to1} + k_A^{2\to0}$ similarly applies for the second A** excited state. (b) Normalized steady-state population densities computed using eq 1 for the various levels (A in black, A* in red, and A** in green) at increasing incident pump intensity simulated for standard erbium activators with λ_P = 980 nm ($^4I_{11/2} \leftarrow {}^4I_{15/2}$) and absorption cross sections $\sigma_A^{0\to1} \approx \sigma_A^{1\to2} = 10^{-20}$ cm^2.[33] The full traces correspond to a fast-relaxing erbium(III) as found in the molecular complex $[GaEr(\mathbf{L1})_3]^{6+}$ with $k_A^{1\to0} = (\tau_{Er^4}^{I_{13/2}})^{-1} = (2.79\ \mu s)^{-1}$, $k_A^{2\to0} = (\tau_{Er,rad^4}^{S_{3/2}})^{-1} = (619\ \mu s)^{-1}$, and $k_A^{2\to0} + k_A^{2\to1} = (\tau_{Er^4}^{S_{3/2}})^{-1} = (38\ ns)^{-1}$.[34] The dashed traces correspond to the slow-relaxing erbium(III) center doped into Gd_2O_2S with $k_A^{1\to0} = (\tau_{Er^4}^{I_{13/2}})^{-1} = (3.7\ ms)^{-1}$, $k_A^{2\to0} = (\tau_{Er,rad^4}^{S_{3/2}})^{-1} = (619\ \mu s)^{-1}$, and $k_A^{2\to0} + k_A^{2\to1} = (\tau_{Er^4}^{S_{3/2}})^{-1} = (560\ \mu s)^{-1}$.[22]

the activator in its different states (ground state $dN_A^{|0\rangle}/dt$, intermediate excited state $dN_A^{|1\rangle}/dt$, and second excited state $dN_A^{|2\rangle}/dt$) can be written in a compact matrix form $[dN_A^{|i\rangle}/dt] = \mathbf{M} \times [N_A^{|i\rangle}]$, which is detailed in eq 1 for the ESA mechanism.[36]

$$\begin{pmatrix} dN_A^{|0\rangle}/dt \\ dN_A^{|1\rangle}/dt \\ dN_A^{|2\rangle}/dt \end{pmatrix} = \begin{pmatrix} -k_A^{exc(0\to1)} & k_A^{1\to0} & k_A^{2\to0} \\ k_A^{exc(0\to1)} & -(k_A^{exc(1\to2)} + k_A^{1\to0}) & k_A^{2\to1} \\ 0 & k_A^{exc(1\to2)} & -(k_A^{2\to0} + k_A^{2\to1}) \end{pmatrix} \begin{pmatrix} N_A^{|0\rangle} \\ N_A^{|1\rangle} \\ N_A^{|2\rangle} \end{pmatrix} \quad (1)$$

While the relaxation rate constants $k_A^{i\to j}$ combine the well-known radiative and nonradiative contributions, which can be approached both theoretically and experimentally,[37] the pumping rate constants $k_A^{exc(i\to j)}$ are given in eq 2, where λ_P is the pump wavelength, P is the incident pump intensity, $\sigma_A^{i\to j}$ is the absorption cross section of the activator-centered $i \to j$ transition, h is the Planck constant, and c is the speed of light in vacuo.[38]

$$k_A^{exc(i\to j)} = \frac{\lambda_P}{hc} P \sigma_A^{i\to j} \quad (2)$$

Under steady-state excitation ($dN_A^{|i\rangle}/dt = 0$), the time-independent population densities in the A, A*, and A** states should be obtained by solving $\mathbf{M} \times [N_{A,s\text{-}s}^{|i\rangle}] = [0]$. However, the conservation of mass for the activator A provides a singular kinetic matrix $\mathbf{M}$, which cannot be inverted. An elegant solution introduces the law of conservation of mass $\sum_{i=0}^{2} N_{A,s\text{-}s}^{|i\rangle} = 1$ as an additional line in the kinetic matrix $\mathbf{M}$, which then becomes rectangular and overdetermined. This format is compatible with the use of linear least-squares methods for extracting the steady-state population densities $N_{A,s\text{-}s}^{|i\rangle}$ as a function of P.[39] Let us stress here that the steady-state population density in the second excited states A** ($N_{A,s\text{-}s}^{|2\rangle}$) is the most interesting one because it is proportional to the intensity of the emitted upconversion (Figure 3a). The normalized population density $N_{A,s\text{-}s}^{|2\rangle}$ computed for long-lived (millisecond range) erbium-centered activators found in bulk solids (dashed traces in Figure 3b) drops by more than 7 orders of magnitude for the molecular system (full traces in Figure 3b), which possesses a microsecond range lifetime for its intermediate excited states, such as, for instance, the Er($^4I_{13/2}$) manifold in an erbium complex. Because these quantitative pessimistic predictions became available only recently,[39] coordination chemists first tried their luck in detecting lanthanide-centered upconversion in their preferred complexes upon high-intensity laser excitation of lanthanide-centered intrashell f → f transitions. A thorough investigation at the beginning of the century focused on the well-known triple-helical $[Ln(dipicolinate)_3]^{3-}$ anionic complexes (Ln = Tm, Er, Yb; Figure 4a), for which downshifted visible Tm($^1G_4 \to {}^3H_6$) at 477 nm (blue) and Tm($^1G_4 \to {}^3H_4$) at 648 nm (red) and near-infrared (NIR) Tm($^3F_4 \to {}^3H_6$) at 809 nm and Yb($^2F_{5/2} \to {}^2F_{7/2}$) at 985 nm luminescence could be detected upon UV ligand excitation.[28] Because of efficient nonradiative deexcitation of the lanthanide excited states by high-energy phonons produced by the vibrations of the organic receptors, the excited-state lifetimes recorded for $[Ln(dipicolinate)]^{3-}$ (Ln = Tm, Yb) did not exceed a few microseconds and no upconversion processes could be evidenced upon NIR laser irradiation of $[Tm(dipicolinate)]^{3-}$ at 807 nm ($^3F_4 \leftarrow {}^3H_6$) or $[Er(dipicolinate)]^{3-}$ at 976 nm ($^4I_{11/2} \leftarrow {}^4I_{15/2}$).[28]

Probably stimulated by the claim that "there is no chance to induce and observe upconversion luminescence in these molecular compounds" explicitly written in the conclusion of ref 28, aqueous solutions of $[Ln(dipicolinate)_3]^{3-}$ (Ln = Er, Tm) were submitted 3 years later to concomitant double NIR (1100−800 nm) laser excitations using huge incident power pump intensities of around 10^9 W cm^{-2}. The latter limitations were indeed broken, and very weak blue Tm($^1G_4 \to {}^3H_6$) and green Er($^4S_{3/2} \to {}^4I_{15/2}$) upconverted signals could be detected; however, no clear rationalization of the mechanism responsible for this success was provided with this work.[40] A reexploration

DOI: 10.1021/acs.inorgchem.6b00700
Inorg. Chem. 2016, 55, 9964−9972

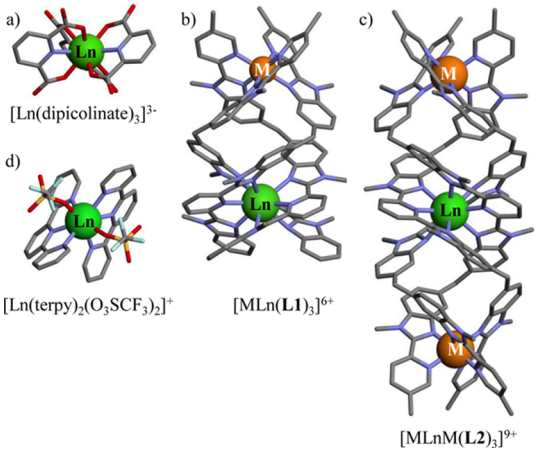

Figure 4. Molecular structures of the complexes (a) $[Ln(dipicolinate)_3]^{3-}$ (taken from the crystal structure of $Na_3[Yb(dipicolinate)_3]\cdot 13H_2O$),[42] (b) $[MLn(\mathbf{L1})_3]^{6+}$ (taken from the crystal structure of $[CrEr(\mathbf{L1})_3](CF_3SO_3)_6\cdot 26C_3H_5N$),[34] (c) $[MLnM(\mathbf{L2})_3]^{9+}$ (taken from the crystal structure of $[GaErGa(\mathbf{L2})_3](CF_3SO_3)_9\cdot 35.5C_2H_3N$),[34] and (d) $[Ln(terpy)2(O_3SCF_3)_2]^+$ (taken from the crystal structure of $[Er(terpy)_2(O_3SCF_3)_2]CF_3SO_3\cdot 1.5C_3H_5N$). See Tables S1−S3 and Figure S1 in the Supporting Information.

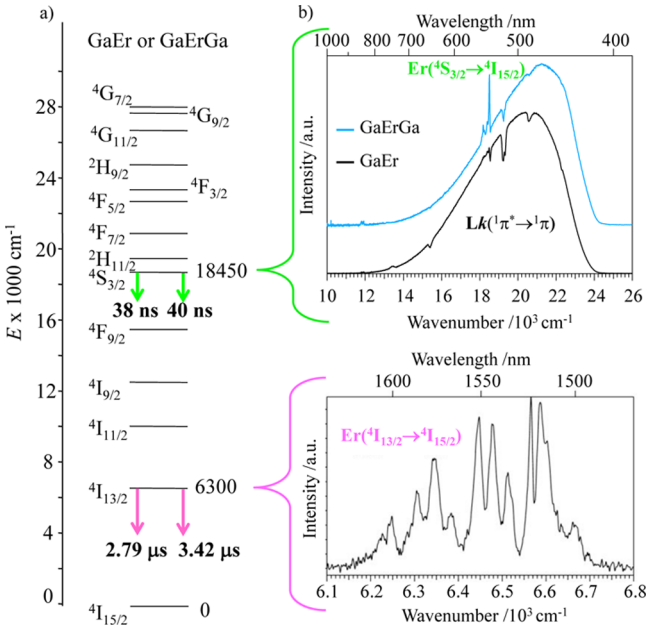

Figure 5. (a) Jablonski diagrams for the $[ErN_9]$ chromophores in $[GaEr(\mathbf{L1})_3](CF_3SO_3)_6$ and $[GaErGa(\mathbf{L2})_3](CF_3SO_3)_9$. The emissive levels are shown with full downward arrows, and their characteristic lifetimes in pure solids at 3−10 K are indicated. (b) Visible (top) and NIR (bottom) luminescence spectra recorded for $[GaEr(\mathbf{L1})_3](CF_3SO_3)_6$ (black trace) and $[GaErGa(\mathbf{L2})_3](CF_3SO_3)_9$ (blue trace) at 3 K in the solid state (λ_{ex} = 405 nm). The dips correspond to internal erbium-centered reabsorption of the broad residual ligand-centered $^1\pi^* \rightarrow {}^1\pi$ emission.[34,39]

of the effect of massive laser irradiation on coordination complexes using a NIR-tunable femtosecond laser (680−1000 nm) demonstrated that even standard solvated $Tm(O_3SCF_3)_3$ in deuterated dimethyl sulfoxide displayed blue $Tm(^1D_2\rightarrow{}^3H_6)$ at 450 nm and $Tm(^1G_4\rightarrow{}^3H_6)$ at 477 nm upconverted emissions.[41] A careful inspection of the upconverted excitation spectrum allowed the authors to conclude that nonlinear two- and three-photon absorption processes dominated the sensitization process under these extreme conditions, while only some minute contribution could be tentatively assigned to linear ESA.[41] In view of the simulations given in Figure 3b, it is a pity that the complexes with highly protected erbium(3+), which were specifically designed for generating long intermediate excited-state lifetimes such as, for instance, perdeuterated cryptates [$\tau_{Er(^4I_{13/2})}$ = 5.7 μs in CD_3CN][43] and perfluorinated iminodiphosphinates [$\tau_{Er(^4I_{13/2})}$ = 741 μs in CD_3CN],[44] were not exposed to NIR excitations for the induction of ESA processes. The reason for this lack of interest for potential molecular upconversion was probably linked to the general belief that trivalent erbium coordinated in molecular complexes possesses only a single, short-lived, and weak emissive state $Er(^4I_{13/2}\rightarrow{}^4I_{15/2})$ in the NIR at 1585 nm with strictly no chance to display upconverted emission.[45] However, when judiciously protected from coupling with high-energy oscillators in the triple-stranded helicates $[GaEr(\mathbf{L1})_3]^{6+}$ and $[GaErGa(\mathbf{L2})_3]^{9+}$ (Figure 4b,c), a second level, namely, the $Er(^4S_{3/2})$ manifold, was found to be emissive. This provided a short-lived green fluorescence detected at 545 nm for the $Er(^4S_{3/2}\rightarrow{}^4I_{15/2})$ transition, together with a standard microsecond NIR $Er(^4I_{13/2}\rightarrow{}^4I_{15/2})$ emission at 1585 nm (Figure 5), a situation that was thought to be exceptional for molecular complexes.[34] In order to substantiate this assertion, we deliberately synthesized mononuclear erbium complexes with vacant coordination sites. Taking the unsaturated complex $[Er(terpy)_2(O_3SCF_3)_2]^+$ as a working example for this forum contribution, its crystal structure highlights the limited protection of the metallic site (Figure 4d), whereas its detailed photophysical characterization (Figure S2 in the Supporting Information) reveals the "unusual" dual erbium-centered luminescence with emissions in the green [$\tau_{Er(^4S_{3/2})}$ = 8.9(4) ns] and in the NIR [$\tau_{Er(^4I_{13/2})}$ = 1.61(1) μs] at 295 K. It thus appears that the existence of a second high-energy emissive excited-state level, as found in $[GaEr(\mathbf{L1})_3]^{6+}$ and $[GaErGa(\mathbf{L2})_3]^{9+}$, is probably much more common than expected. However, this condition does not represent a guarantee for programming molecular-based ESA and NIR excitation of these complexes in the 690−780 nm range with an incident pump intensity P = 10−500 W cm^{-2} did not produce any upconverted signals.[39]

To the best of our knowledge, there is until now no definitive proof of the observation of a lanthanide-centered ESA mechanism produced by the linear double excitation of a coordination complex using a reasonable incident pump power intensity (10−500 W cm^{-2}). An efficient protection of the metallic center from sources of nonradiative deactivation located on ligands (fluorination or deuteration of these surrounding ligands), which maximizes the lifetime of the intermediate excited state, appears to be a promising strategy for both Ln = Tm and Er activators.

MULTICENTER SUPEREXCITATION IN MOLECULAR COMPLEXES: THE ETU MECHANISM

The upconverted intensity I_{up}^{ESA} produced by single-ion ESA under steady-state conditions can be summarized by eq 3, which corresponds to the algebraic solution of eq 1.

DOI: 10.1021/acs.inorgchem.6b00700
Inorg. Chem. 2016, 55, 9964−9972

$$I_{up}^{ESA} \propto N_{A,s\text{-}s}^{|2\rangle}(ESA) = \left(\frac{\lambda_p}{hc}\right)^2 P^2 \times \frac{\sigma_A^{0\to1}\sigma_A^{1\to2}}{(k_A^{2\to1} + k_A^{2\to0})[k_A^{1\to0} + (\lambda_p/hc)P\sigma_A^{1\to2}]} N_{A,s\text{-}s}^{|0\rangle} \quad (3)$$

The situation appears more complicated for multiple-ion ETU when the activator undergoes successive indirect excitations via energy transfer from the sensitizers (Figure 6).

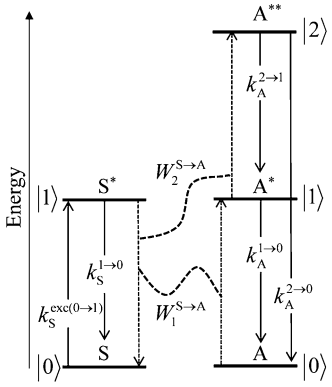

Figure 6. Kinetic scheme depicting the modeling of a sensitizer−activator ETU process occurring upon off-resonance irradiation into the sensitizer-centered absorption band. $k_A^{1\to0}$ stands for the global decay rate constant of the first A* excited state, and $k_A^{2\to1} + k_A^{2\to0}$ similarly applies for the second A** excited state. $k_S^{1\to0}$ is the deactivation rate constant of the sensitizer excited state S* in the absence of energy transfer, and $W^{S\to A}$ are the intermolecular second-order rate constants for sensitizer-to-activator energy transfer.

Because the ETU pathway involves second-order kinetic processes, the associated upconverted intensity I_{up}^{ETU} depends on the concentrations of both the activator and sensitizer, as shown in eq 4.[46] However, both the ESA and ETU mechanisms will become very unfavorable for fast-relaxing activators because the relaxation rate constant of the intermediate excited state A* ($k_A^{1\to0}$) contributes to the reduction of both I_{up}^{ESA} (eq 3) and I_{up}^{ETU} (eq 4).[46]

$$I_{up}^{ETU} \propto N_{A,s\text{-}s}^{|2\rangle}(ETU) = \left(\frac{\lambda_p}{hc}\right)^2 P^2 \times \frac{(\sigma_S^{0\to1})^2 W_1^{S\to A} W_2^{S\to A} (N_{S,s\text{-}s}^{|0\rangle})^2}{(k_A^{2\to1} + k_A^{2\to0}) k_{S,obs}^{1\to0} (k_A^{1\to0} k_{S,obs}^{1\to0} + (\lambda_p/hc)P\sigma_S^{0\to1} W_2^{S\to A} N_{S,s\text{-}s}^{|0\rangle})} N_{A,s\text{-}s}^{|0\rangle}$$

$$\text{with } k_{S,obs}^{1\to0} = k_S^{1\to0} + W_1^{S\to A} N_{A,s\text{-}s}^{|0\rangle} \quad (4)$$

For reasonable incident pump power intensities, the major fraction of the activator and sensitizer ions remains in the ground state under the steady-state illumination regime (i.e., $N_{A,s\text{-}s}^{|0\rangle} \approx N_{A,s\text{-}s}^{tot}$ and $N_{S,s\text{-}s}^{|0\rangle} \approx N_{S,s\text{-}s}^{tot}$), and the gain of the ETU mechanism (Figure 6) over the ESA mechanism (Figure 3) is given by eq 5.[46]

$$\frac{N_{A,s\text{-}s}^{|2\rangle}(ETU)}{N_{A,s\text{-}s}^{|2\rangle}(ESA)} = \frac{(\sigma_S^{0\to1})^2}{\sigma_A^{0\to1}\sigma_A^{1\to2}} \frac{W_1^{S\to A} W_2^{S\to A} (N_{S,s\text{-}s}^{tot})^2}{(k_S^{1\to0} + W_1^{S\to A} N_{A,s\text{-}s}^{tot})^2} = \frac{(\sigma_S^{0\to1})^2}{\sigma_A^{0\to1}\sigma_A^{1\to2}} \frac{W_1^{S\to A} W_2^{S\to A}}{(k_{S,obs}^{1\to0})^2} (N_{S,s\text{-}s}^{tot})^2 \quad (5)$$

On the right-hand side of eq 5, the first ratio denotes the advantage that results from the use of sensitizers possessing larger absorption cross sections with respect to those of the lanthanide activators ($\sigma_S^{0\to1} \gg \sigma_A^{j\to j}$). The central ratio is maximized when two efficient S → A energy-transfer processes are combined with a sensitizer possessing a long lifetime in its excited state S*. Please note that $W_1^{S\to A}$ contributes to both the numerator and denominator (via $k_{S,obs}^{1\to0} = k_S^{1\to0} + W_1^{S\to A} N_{A,s\text{-}s}^{|0\rangle}$) in eq 5, which implies some judicious tuning of this parameter. Finally, the ETU mechanism depends on the square of the concentration of the sensitizer $(N_{S,s\text{-}s}^{tot})^2$, which explains the improvement commonly observed upon going from ESA to ETU in doped bulk solids and nanoparticles.[12−15] Related relative enhancement is expected in multimetallic-doped polymeric systems containing fast-relaxing lanthanide ions, and the ETU mechanism has thus been invoked for rationalization of the simultaneous blue Er($^2H_{9/2}\to{}^4I_{15/2}$), green Er($^4S_{3/2}\to{}^4I_{15/2}$), and red Er($^4F_{9/2}\to{}^4I_{15/2}$) visible emissions detected in an Y:Yb−Er-codoped lanthanide−organic framework upon laser irradiation into the Yb($^2F_{7/2}\to{}^2F_{5/2}$) transition at 975 nm.[47] A more surprising cooperative upconversion mechanism is thought to involve quasi-virtual pair levels, between which transitions have to be described at a higher order of perturbation because of their double-operator nature, to explain the sensitization of Tb($^5D_4\leftarrow{}^7F_6$) or Eu($^5D_1\leftarrow{}^7F_0$) emissions from two excited ytterbium(3+) ions in codoped perfluorobutanesulfonate polymers.[48] The harsh treatment applied to the latter polymeric material (570 K at 10^{-5} Pa for 3 weeks) prior to performing photophysical investigations casts some doubt on the exact nature of the lanthanide coordination spheres in these samples.

Returning to fast-relaxing lanthanide activators lying in molecular complexes, the sensitizer and activator belong to the same discrete object, and the intermolecular S → A energy-transfer processes pertinent to doped solids (Figure 6) transform into intramolecular processes. This removes the dependence on the sensitizer concentration (Figure 7a). Consequently, a considerable part of the beneficial effect predicted for the ETU mechanism operating in doped solids or polymers (eq 5) is not relevant to SA pairs found in molecules [compare the full green (ETU) to the full blue (ESA) traces in Figure 7b].[39] It is therefore not so surprising that coordination chemists tried to exploit the remaining specific advantage brought by a large absorption coefficient on the sensitizer for inducing detectable upconversion in molecules.

A first intriguing result was reported in 2003 by Hoshino and co-workers, who focused an intense laser beam at 514.5 nm in the low-energy tail of the ligand absorption band of a vacuum-deposited thin film of [Er(quinolinate)$_3$].[50] The induced blue-green erbium-centered upconverted emission suggests the operation of an ETU mechanism using the ligand as the sensitizer and the erbium as the activator, but its alternative assignment to a ligand-centered NLO two-photon sensitization followed by energy transfer onto the trivalent erbium cation cannot be excluded. The same strategy was followed for an [Er(TTA)$_4$](IR806) ion pair (Figure 8a), in which the organic dye IR806 was submitted to NIR excitation at 808 nm. A convincing green Er($^2H_{11/2}\to{}^4I_{15/2}$) + Er($^4S_{3/2}\to{}^4I_{15/2}$) ETU emission could be detected in anhydrous deuterated chloroform (Figure 8b).[51] A breakthrough in the field of upconversion operating in molecular complexes occurred when Aboshyan-Sorgho et al. realized that the introduction of

DOI: 10.1021/acs.inorgchem.6b00700
Inorg. Chem. 2016, 55, 9964−9972

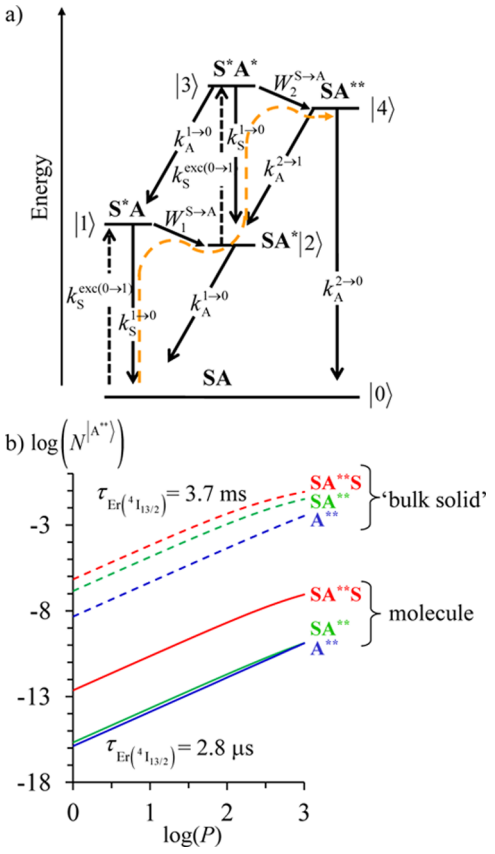

Figure 7. (a) Kinetic scheme depicting the modeling of an ETU process occurring upon off-resonance irradiation into the sensitizer-centered absorption band in a molecular SA pair. The orange dashed trace highlights the ETU mechanism. (b) log–log plots of the computed upconverted emission intensity as a function of the incident pump power intensity (P in W cm^{-2}) computed for ESA for a single erbium center in $[GaEr(\mathbf{L1})_3]^{6+}$ (blue traces; A = Er = activator) and ETU for a molecular CrEr pair in $[CrEr(\mathbf{L1})_3]^{6+}$ (green traces, S = Cr = sensitizer) and a molecular triad CrErCr in $[CrErCr(\mathbf{L2})_3]^{9+}$ (red traces).[49] The full traces correspond to the fast-relaxing erbium(III) center found in these complexes [$\tau_{Er(^4I_{13/2})}$ = 2.8 μs]. The dashed traces correspond to a virtual slow-relaxing erbium(III) in the same complexes [$\tau_{Er(^4I_{13/2})}$ = 3.7 ms].[49]

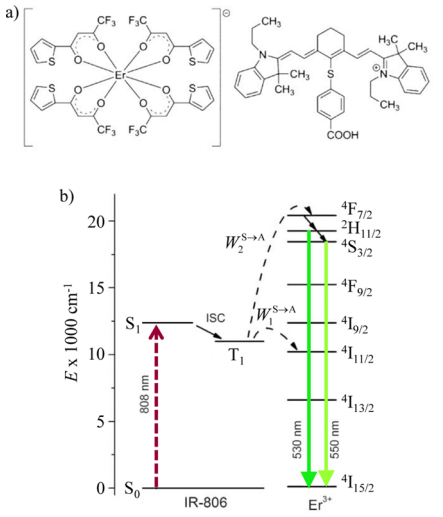

Figure 8. (a) Chemical structure of the $[Er(TTA)_4](IR806)$ ion pair and (b) Jablonski diagram showing the proposed ETU mechanism operating in $[Er(TTA)_4](IR806)$ ($CDCl_3$ at room temperature). Adapted from ref 51.

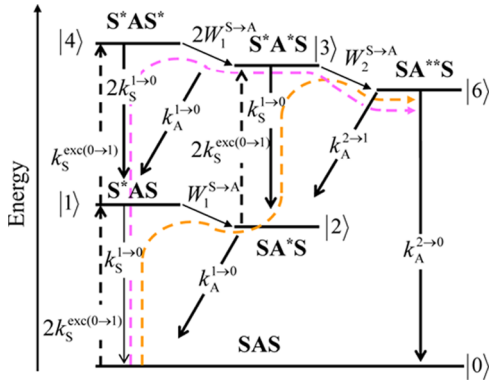

Figure 9. Partial kinetic scheme depicting the modeling of an ETU process occurring upon off-resonance irradiation into the sensitizer absorption band in a discrete SAS triad ($W_1^{S\to A}$ and $W_2^{S\to A}$ are the first-order rate constants for the successive S → A energy transfers). The orange and pink dashed traces highlight the two mechanisms contributing to the ETU.[49]

a second sensitizer in a SAS triad opened a novel pathway for upconversion (dashed pink arrow in Figure 9).[52]

The "standard" activator-centered ETU pathway operating in both discrete SA pairs and SAS triads (dashed orange traces in Figures 7a and 9) is expected to become 2^2 = 4 times more efficient in the SAS triad because two sensitizers (instead of one in SA) are statistically excited to reach the successive S*AS and S*A*S excited-state levels (this situation is equivalent to the quadratic dependence on the sensitizer concentration predicted in doped materials in eq 4). The "novel" sensitizer-centered pathway implemented in the SAS triad (dashed pink trace in Figure 9) brings a more efficient mechanism for upconversion because it prevents the deleterious competition between the fast A-centered relaxation ($k_A^{1\to0}$) and the slow S-centered excitation ($k_S^{exc(0\to1)}$), which occurs in the intermediate SA*S excited-state level (Figure 9).[39] The numerical simulation of upconverted emission under steady-state excitation for a SA pair (green traces in Figure 7b) and for a C_2-symmetrical SAS triad (red traces in Figure 7b) predicts that the addition of a second sensitizer into a coordination complex containing a fast-relaxing lanthanide activator may improve the upconverted intensity by 3 orders of magnitude (full traces in Figure 7b). This effect levels out with slow-relaxing activators, as those found in nanoparticles (dashed traces in Figure 7b). The D_3-symmetrical triple-stranded helicate $[CrErCr(\mathbf{L2})_3](CF_3SO_3)_9$ was designed for optimization of ETU upconversion in a CrErCr triad (Figure 10a).[39,52] The considerable intermetallic separation distance (~9 Å) combined with the absence of bridging atoms between the metallic cations in the trinuclear helicate $[CrErCr(\mathbf{L2})_3]^{9+}$ restricts the intramolecular Cr → Er energy-transfer processes to weak multipolar electric interactions characterized by $\eta_1^{S\to A} = W_1^{S\to A}/k_{S,obs}^{1\to0}$ ~ 30% efficiency,[34] thus ensuring an intermediate $Cr(^2E)$ excited-state lifetime long enough (in the millisecond range) for maximizing the beneficial contribution of the sensitizer-centered ETU mechanism. Irradiation into the $Cr(^2T_1 \leftarrow {}^4A_2)$ transition at 715 nm for $[CrErCr(\mathbf{L2})_3]^{9+}$ in frozen acetonitrile solutions (4–150 K) or in solid-state solutions (4–293 K; 2% or 10% diluted in $[GaYGa(\mathbf{L2})_3](CF_3SO_3)_9$) induced molecular-based upconverted green $Er(^4S_{3/2} \rightarrow {}^4I_{15/2})$ emissions (dark-green trace in

DOI: 10.1021/acs.inorgchem.6b00700
Inorg. Chem. 2016, 55, 9964–9972

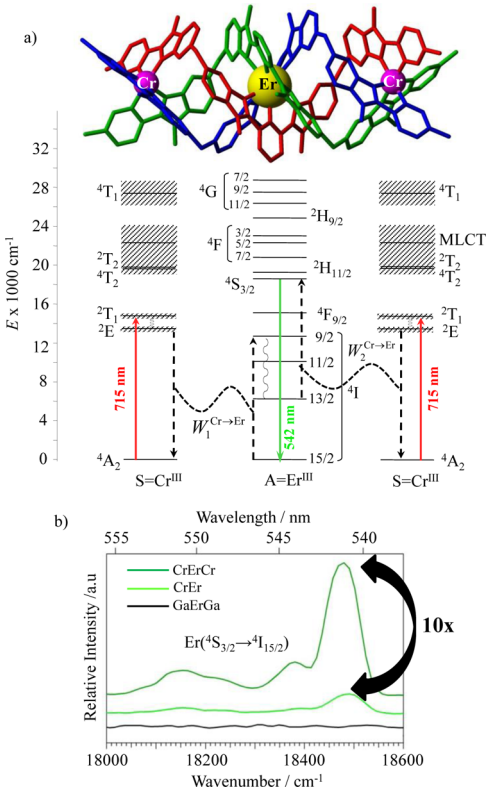

Figure 10. (a) Jablonski diagrams obtained from the absorption and emission spectra recorded for the different chromophores in $[CrErCr(\mathbf{L2})_3](CF_3SO_3)_9$. Black dashed arrows indicate radiationless sensitizer-to-activator energy-transfer processes, and curled arrows stand for nonradiative internal conversion. Red solid arrows correspond to the NIR excitation photons, and the green solid arrow stands for the visible upconverted emission. (b) Green upconverted $Er(^4S_{3/2}\rightarrow{}^4I_{15/2})$ emissions observed for $[CrErCr(\mathbf{L2})_3](CF_3SO_3)_9$ and $[CrEr(\mathbf{L1})_3](CF_3SO_3)_6$ in frozen solution [10 mM in acetonitrile/propionitrile (4:1), 31 K, λ_{exc} = 715 nm, and $P \approx 1$ W mm^{-2}].[39] The reference sample with gallium replacing chromium, $[GaErGa(\mathbf{L2})_3](CF_3SO_3)_9$, shows no luminescence under the same experimental conditions.

Figure 10b).[39] In an effort to support the kinetic schemes established in Figures 7a and 9, the analogous binuclear helicate $[CrEr(\mathbf{L1})_3](CF_3SO_3)_6$ (see Figure 4b for its molecular structure) was similarly irradiated at 715 nm to generate a much weaker upconverted signal (light-green trace in Figure 10b). Detailed simulations using the experimental rate constants obtained for both CrEr and CrErCr helicates predict that the intensity of the upconverter emission should be reduced by 1 order of magnitude in the binuclear helicate,[34] a result in line with the experimental value of a 4−12 times decrease of the upconverted $Er(^4S_{3/2}\rightarrow{}^4I_{15/2})$ luminescence recorded for $[CrEr(\mathbf{L1})_3]^{6+}$ under various experimental conditions.[39]

CONCLUSION

Because of the high probability of the fast nonradiative relaxation of excited states in coordination complexes, lanthanide-centered molecular upconversion has been considered for a long period to be impossible.[28] Theoretical predictions, however, suggest that this ban can be overcome if sufficiently long-lived intermediate excited states can be generated in lanthanide complexes. Unfortunately, the best protected trivalent erbium cations possessing long excited-state lifetimes in coordination complexes have not been submitted to ESA experiments to date.[43,44] It is therefore difficult to establish the lower limit of incident pumping intensities required for inducing a detectable single-ion excitation at the molecular level. For the systems studied so far, huge pumping intensities (on the order of several MW cm^{-2}) have been used for generating upconverted signals, and it was difficult to differentiate between linear or nonlinear processes. We have, however, no doubt that trivalent erbium or thulium cations encapsulated in low-phonon fluorinated/deuterated environments will soon lead to the first undeniable reports of molecular ESA upconversion in coordination complexes under reasonable excitation powers. In line with the original reasoning applied for bulk solids,[11] indirect excitation via ETU benefits from the larger absorption cross section of the sensitizer, particularly when the latter is an organic dye such as for the $[Er(TTA)_4](IR806)$ ion pair (Figure 8).[51] Interestingly, the replacement of intermolecular energy-transfer processes as observed in multiple-ion-codoped solids,[53] with directional intramolecular processes operating in S_nA molecular complexes, results in the separation of the ETU pathway into two parts. First, the activator-centered mechanism exists for $n \geq 1$ and its efficiency increases as n^2. It is the only one available in a SA pair (Figure 7a). The alternative sensitizer-centered mechanism works only for $n \geq 2$, and its efficiency increases as $n(n-1)$. This second mechanism can be optimized by a judicious choice of sensitizers, which must possess sufficiently long-lived excited states despite the presence of efficient S → A energy transfer. To the best of our knowledge, the CrEr and CrErCr helicates shown in Figure 10 are currently the only systems for which these predictions have been investigated and confirmed. It is clear that molecular lanthanide-centered upconversion is still in its infancy today and, in paraphrasing Feynman,[54] "there is plenty room at the bottom" for some further miniaturization of upconverting materials, with the molecular aspects probably being of crucial importance in this respect.

ASSOCIATED CONTENT

Supporting Information

The Supporting Information is available free of charge on the ACS Publications website at DOI: 10.1021/acs.inorgchem.6b00700.

Experimental details, tables of crystal data and geometric parameters, and figures showing molecular structures, emission spectra, and kinetic matrixes (PDF)

CIF file for $[Er(terpy)_2(O_3SCF_3)_2](CF_3SO_3)\cdot 1.5C_3H_5N$ (CIF)

AUTHOR INFORMATION

Corresponding Author

*E-mail: Claude.Piguet@unige.ch.

Notes

The authors declare no competing financial interest.

ACKNOWLEDGMENTS

Financial support from the Swiss National Science Foundation is gratefully acknowledged. S.P. aknowledges support from La Ligue contre le Cancer, Cancéropôle Grand Ouest and INSERM.

DOI: 10.1021/acs.inorgchem.6b00700
Inorg. Chem. 2016, 55, 9964−9972

REFERENCES

(1) (a) Kerr, J. *Philos. Mag. S.* **1875**, *50*, 337−348. (b) Crova, A. *J. Phys. Theor. Appl.* **1879**, *8*, 414−418.
(2) Goeppert-Mayer, M. *Ann. Phys.* **1931**, *401*, 273−294.
(3) Franken, P. A.; Hill, A. E.; Peters, C. W.; Weinreich, G. *Phys. Rev. Lett.* **1961**, *7*, 118−119.
(4) Kaiser, W.; Garrett, C. G. B. *Phys. Rev. Lett.* **1961**, *7*, 229−231.
(5) Maiman, T. H. *Nature* **1960**, *187*, 493−494.
(6) (a) He, G. S.; Tan, L.-S.; Zheng, Q.; Prasad, P. N. *Chem. Rev.* **2008**, *108*, 1245−1330. Terenziani, F.; Katan, C.; Badaeva, E.; Tretiak, S.; Blanchard-Desce, M. *Adv. Mater.* **2008**, *20*, 4641−4678.
(7) Andraud, C.; Maury, O. *Eur. J. Inorg. Chem.* **2009**, *2009*, 4357−4371.
(8) (a) Neveu, P.; Aujard, I.; Benbrahim, C.; Le Saux, T.; Allemand, J.-F.; Vriz, S.; Bensimon, D.; Jullien, L. *Angew. Chem., Int. Ed.* **2008**, *47*, 3744−3746. (b) Sinha, D. K.; Neveu, P.; Gagey, N.; Aujard, I.; Benbrahim-Bouzidi, C.; Le Saux, T.; Rampon, C.; Gauron, C.; Goetz, B.; Dubruille, S.; Baaden, M.; Volovitch, M.; Bensimon, D.; Vriz, S.; Jullien, L. *ChemBioChem* **2010**, *11*, 653−663.
(9) (a) D'Aléo, A.; Bourdolle, A.; Brustlein, S.; Fauquier, T.; Grichine, A.; Duperray, A.; Baldeck, P. L.; Andraud, C.; Brasselet, S.; Maury, O. *Angew. Chem., Int. Ed.* **2012**, *51*, 6622−6625. (b) Soulié, M.; Latzko, F.; Bourrier, E.; Placide, V.; Butler, S. J.; Pal, R.; Walton, J. W.; Baldeck, P. L.; Le Guennic, B.; Andraud, C.; Zwier, J. M.; Lamarque, L.; Parker, D.; Maury, O. *Chem. - Eur. J.* **2014**, *20*, 8636−8646. (c) Bui, A. T.; Grichine, A.; Brasselet, S.; Duperray, A.; Andraud, C.; Maury, O. *Chem. - Eur. J.* **2015**, *21*, 17757−17761.
(10) Bloembergen, N. *Phys. Rev. Lett.* **1959**, *2*, 84−85.
(11) (a) Gamelin, D. R.; Güdel, H. U. *Acc. Chem. Res.* **2000**, *33*, 235−242. (b) Auzel, F. *Chem. Rev.* **2004**, *104*, 139−173. (c) van der Ende, B. M.; Aarts, L.; Meijerink, A. *Phys. Chem. Chem. Phys.* **2009**, *11*, 11081−11095. (d) Zhou, J.; Liu, Q.; Feng, W.; Sun, Y.; Li, F. *Chem. Rev.* **2015**, *115*, 395−465.
(12) (a) Auzel, F. *C. R. Acad. Sci. Paris* **1966**, *B262*, 1016−1019. (b) Auzel, F. *C. R. Acad. Sci. Paris* **1966**, *B263*, 819−821.
(13) Wright, J. Up-conversion and excited-state energy transfer in rare-earth doped materials. In *Radiationless Processes in Molecules and Condensed Phases*; Fong, F. K., Ed.; Topics in Applied Physics; Springer: New York. 1976; Vol. *15*, p 239.
(14) (a) Liu, G. *Chem. Soc. Rev.* **2015**, *44*, 1635−1652. (b) Dong, H.; Sun, L.-D.; Yan, C.-H. *Chem. Soc. Rev.* **2015**, *44*, 1608−1634. (c) Liu, X.; Qiu, J. *Chem. Soc. Rev.* **2015**, *44*, 8714−8746.
(15) (a) Wang, F.; Liu, X. *Chem. Soc. Rev.* **2009**, *38*, 976−989. (b) Haase, M.; Schäfer, H. *Angew. Chem., Int. Ed.* **2011**, *50*, 5808−5829. (c) Chen, G.; Yang, C.; Prasad, P. N. *Acc. Chem. Res.* **2013**, *46*, 1474−1486. (d) Wang, F.; Liu, X. *Acc. Chem. Res.* **2014**, *47*, 1378−1385. (e) Liu, X.; Qiu, J. *Chem. Soc. Rev.* **2015**, *44*, 8714−8746.
(16) (a) Strohhofer, C.; Polman, A. *J. Appl. Phys.* **2001**, *90*, 4314−4320. Kik, P. G.; Polman, A. *J. Appl. Phys.* **2003**, *93*, 5008−5012.
(17) (a) Zhao, J.; Jin, D.; Schartner, E. P.; Lu, Y.; Liu, Y.; Zvyagin, A. V.; Zhang, L.; Dawes, J. M.; Xi, P.; Piper, J. A.; Goldys, E. M.; Monro, T. M. *Nat. Nanotechnol.* **2013**, *8*, 729−734.
(18) (a) Lenth, W.; Macfarlane, R. M. *J. Lumin.* **1990**, *45*, 346−350. (b) Lenth, W.; Macfarlane, R. M. *Opt. Photonics News* **1992**, *3*, 8−15. (c) Joubert, M. F.; Guy, S.; Jacquier, B. *Phys. Rev. B: Condens. Matter Mater. Phys.* **1993**, *48*, 10031−10037. (d) Scheps, R. *Prog. Quantum Electron.* **1996**, *20*, 271−358. (e) Downing, E.; Hesselink, L.; Ralston, J.; Macfarlane, R. M. *Science* **1996**, *273*, 1185−1189.
(19) Huang, X.; Han, S.; Huang, W.; Liu, X. *Chem. Soc. Rev.* **2013**, *42*, 173−201. Ramasamy, P.; Manivasakan, P.; Kim, J. Y. *RSC Adv.* **2014**, *4*, 34873−34895. (c) Bünzli, J.-C. G.; Chauvin, A.-S. Lanthanides in Solar Energy Conversion. In *Handbook on the Physics and Chemistry of Rare Earths*; Bünzli, J.-C. G., Pecharsky, V. K., Eds.; Elsevier North Holland: Amsterdam, The Netherlands, 2014; Vol. *44*, pp 169−281.
(20) (a) Liu, Y.; Tu, D.; Zhu, H.; Chen, X. *Chem. Soc. Rev.* **2013**, *42*, 6924−6958. (b) Chen, G.; Qiu, H.; Prasad, P. N.; Chen, X. *Chem. Rev.* **2014**, *114*, 5161−5214. (c) Gai, S.; Li, C.; Yang, P.; Lin, J. *Chem. Rev.* **2014**, *114*, 2343−2389. (d) Sun, L.-D.; Wang, Y.-F.; Yan, C.-H. *Acc. Chem. Res.* **2014**, *47*, 1001−1009.
(21) (a) Pansare, V. J.; Hejazi, S.; Faenza, W. J.; Prud'homme, R. K. *Chem. Mater.* **2012**, *24*, 812−827. (b) Rodriguez Burbano, D. C.; Naccache, R.; Capobianco, J. A. Near-IR Triggered Photon Upconversion: Imaging, Detection, and Therapy. In *Handbook on the Physics and Chemistry of Rare Earths*; Gschneidner, K. A., Jr., Bünzli, J.-C. G., Pecharsky, V. K., Eds.; Elsevier Science: Amsterdam, The Netherlands, 2015; Vol. *47*, pp 273−352.
(22) Martin-Rodriguez, R.; Fischer, S.; Ivaturi, A.; Froehlich, B.; Krämer, K. W.; Goldschmidt, J. C.; Richards, B. S.; Meijerink, A. *Chem. Mater.* **2013**, *25*, 1912−1921.
(23) Page, R.; Schaffers, K.; Waide, P.; Tassano, J.; Payne, S.; Krupke, W.; Bischel, W. *J. Opt. Soc. Am. B* **1998**, *15*, 996−1008.
(24) Wang, F.; Wang, J.; Liu, X. *Angew. Chem., Int. Ed.* **2010**, *49*, 7456−7460.
(25) Boyer, J.-C.; van Veggel, F. C. J. M. *Nanoscale* **2010**, *2*, 1417−1419.
(26) Strohhöfer, C.; Polman, A. *Opt. Mater.* **2003**, *21*, 705−712.
(27) (a) Han, S.; Deng, R.; Xie, X.; Liu, X. *Angew. Chem., Int. Ed.* **2014**, *53*, 11702−11715. (b) Wu, D. M.; Garcia-Etxarri, A.; Salleo, A.; Dionne, J. A. *J. Phys. Chem. Lett.* **2014**, *5*, 4020−4031.
(28) Reinhard, C.; Güdel, H. U. *Inorg. Chem.* **2002**, *41*, 1048−1055.
(29) Lower, S. K.; El-Sayed, M. A. *Chem. Rev.* **1966**, *66*, 199−241.
(30) (a) Parker, C. A.; Hatchard, C. G. *Proc. Chem. Soc.* **1962**, 386−387. (b) Parker, C. A. *Proc. R. Soc. London, Ser. A* **1963**, *276*, 125−135.
(31) $\sigma\ [\mathrm{cm}^2] = (1000\ \ln(10)/N_{AV})\varepsilon\ [\mathrm{M}^{-1}\ \mathrm{cm}^{-1}] \Rightarrow \sigma = 3.82 \times 10^{-21}\varepsilon$. See: Schmidt, T. W.; Castellano, F. N. *J. Phys. Chem. Lett.* **2014**, *5*, 4062−4072.
(32) (a) Singh-Rachford, T. N.; Castellano, F. N. *Coord. Chem. Rev.* **2010**, *254*, 2560−2573. (b) Zhao, J.; Ji, S.; Guo, H. *RSC Adv.* **2011**, *1*, 937−950. (c) Monguzzi, A.; Tubino, R.; Hoseinkhani, S.; Campione, M.; Meinardi, F. *Phys. Chem. Chem. Phys.* **2012**, *14*, 4322−4332. (d) Huang, X.; Han, S.; Huang, W.; Liu, X. *Chem. Soc. Rev.* **2013**, *42*, 173−201. (e) Gray, V.; Dzebo, D.; Abrahamsson, M.; Albinsson, B.; Moth-Poulsen, K. *Phys. Chem. Chem. Phys.* **2014**, *16*, 10345−10352.
(33) Prudenzano, F.; Mescia, L.; Allegretti, L.; Moizan, V.; Nazabal, V.; Smektala, F. *Opt. Mater.* **2010**, *33*, 241−245.
(34) Zare, D.; Suffren, Y.; Guénée, L.; Eliseeva, S. V.; Nozary, H.; Aboshyan-Sorgho, L.; Petoud, S.; Hauser, A.; Piguet, C. *Dalton Trans.* **2015**, *44*, 2529−2540.
(35) For the sake of simplicity, each relaxation rate constant corresponds to the sum of the radiative and nonradiative contributions.
(36) Starzak, M. E. *Mathematical Methods in Chemistry and Physics*; Plenum Press: New York, 1989; pp 289−357.
(37) Bünzli, J.-C. G.; Eliseeva, S. V. Photophysics of Lanthanoid Coordination Compounds. *Comprehensive Inorganic Chemistry II*; Elsevier Ltd.: Amsterdam, The Netherlands, 2013; Vol. *8.08*, pp 340−398.
(38) Pollnau, M.; Gamelin, D. R.; Lüthi, S. R.; Güdel, H. U.; Hehlen, M. P. *Phys. Rev. B: Condens. Matter Mater. Phys.* **2000**, *61*, 3337−3346.
(39) Suffren, Y.; Zare, D.; Eliseeva, S. V.; Guénée, L.; Nozary, H.; Lathion, T.; Aboshyan-Sorgho, L.; Petoud, S.; Hauser, A.; Piguet, C. *J. Phys. Chem. C* **2013**, *117*, 26957−26963.
(40) Xiao, X.; Haushalter, J. P.; Faris, G. W. *Opt. Lett.* **2005**, *30*, 1674−1676.
(41) Blackburn, O. A.; Tropiano, M.; Sorensen, T. J.; Thom, J.; Beeby, A.; Bushby, L. M.; Parker, D.; Natrajan, L. S.; Faulkner, S. *Phys. Chem. Chem. Phys.* **2012**, *14*, 13378−13384.
(42) Albertsson, J.; Nicholson, D. G.; Mukherjee, A. D.; Nilsson, K.; Nimmich, W. *Acta Chem. Scand.* **1972**, *26*, 985−1004.
(43) Doffek, C.; Alzakhem, N.; Molon, M.; Seitz, M. *Inorg. Chem.* **2012**, *51*, 4539−4545.
(44) Glover, P. B.; Bassett, A. P.; Nockemann, P.; Kariuki, B. M.; Van Deun, R.; Pikramenou, Z. *Chem. - Eur. J.* **2007**, *13*, 6308−6320.
(45) (a) Hofstraat, J. W.; Wolbers, M. P. O.; Van Veggel, F. C. J. M.; Reinhoudt, D. N.; Werts, M. H. V.; Verhoeven, J. W. *J. Fluoresc.* **1998**, *8*, 301−308. (b) Artizzu, F.; Mercuri, M. L.; Serpe, A.; Deplano, P. *Coord. Chem. Rev.* **2011**, *255*, 2514−2529.

DOI: 10.1021/acs.inorgchem.6b00700
Inorg. Chem. 2016, 55, 9964−9972

(46) Aboshyan-Sorgho, L.; Cantuel, M.; Petoud, S.; Hauser, A.; Piguet, C. *Coord. Chem. Rev.* **2012**, *256*, 1644−1663.
(47) Sun, C.-Y.; Zheng, X.-J.; Chen, X.-B.; Jin, L.-P.; Li, L.-C. *Inorg. Chim. Acta* **2009**, *362*, 325−330.
(48) Hernandez, I.; Pathumakanthar, N.; Wyatt, P. B.; Gillin, W. P. *Adv. Mater.* **2010**, *22*, 5356−5360.
(49) The full kinetic scheme and associated matrix used for solving $[dN_A^{\langle i \rangle}/dt] = \mathbf{M} \times [N_A^{\langle i \rangle}] = 0$ under steady-state excitation for a SA pair are given in Figure S3, and those for the SAS triad are given in Figure S4 in the Supporting Information. Full traces were simulated using λ_P = 705 nm $[Cr(^2E \leftarrow {}^4A_2)]$ with an absorption cross section of $\sigma_S^{0\rightarrow 1} = 10^{-23}$ m^2, $k_S^{1\rightarrow 0} = (\tau_{Cr\ in\ CrY}^{1\rightarrow 0})^{-1} = (2767\ \mu s)^{-1}$, $k_A^{1\rightarrow 0} = (\tau_{Er}^{^4I_{13/2}})^{-1} = (2.78\ \mu s)^{-1}$, $k_A^{2\rightarrow 0} = (\tau_{Er,rad}^{^4S_{3/2}})^{-1} = (619\ \mu s)^{-1}$, $k_A^{2\rightarrow 0} + k_A^{2\rightarrow 1} = (\tau_{Er^4}^{S_{3/2}})^{-1} = (38$ ns$)^{-1}$, $W_1^{S\rightarrow A} = (\tau_{Cr\ in\ CrEr}^{1\rightarrow 0})^{-1} - (\tau_{Cr\ in\ CrY}^{1\rightarrow 0})^{-1} = 295$ s^{-1}, $W_1^{S\rightarrow A} = 295$ s^{-1}, and $W_2^{S\rightarrow A}$ is arbitrarily fixed to 10^4 s^{-1}. Dashed traces were simulated using the same rate constants except for $k_A^{1\rightarrow 0} = (\tau_{Er^4}^{I_{13/2}})^{-1} = (3.7$ ms$)^{-1}$, $k_A^{2\rightarrow 0} = (\tau_{Er,rad^4}^{S_{3/2}})^{-1} = (619\ \mu s)^{-1}$, $k_A^{2\rightarrow 0} + k_A^{2\rightarrow 1} = (\tau_{Er^4}^{S_{3/2}})^{-1} = (560\ \mu s)^{-1}$.
(50) Suzuki, H.; Nishida, Y.; Hoshino, S. *Mol. Cryst. Liq. Cryst.* **2003**, *406*, 27−37.
(51) Hyppänen, I.; Lahtinen, S.; Ääritalo, T.; Mäkelä, J.; Kankare, J.; Soukka, T. *ACS Photonics* **2014**, *1*, 394−397.
(52) Aboshyan-Sorgho, L.; Besnard, C.; Pattison, P.; Kittilstved, K. R.; Aebischer, A.; Bünzli, J.-C. G.; Hauser, A.; Piguet, C. *Angew. Chem., Int. Ed.* **2011**, *50*, 4108−4112.
(53) Inokuti, M.; Hirayama, F. *J. Chem. Phys.* **1965**, *43*, 1978−1989.
(54) Drexler, E. *There's Plenty of Room at the Bottom*, http://metamodern.com/2009/12/29/theres-plenty-of-room-at-the-bottom%E2%80%9D-feynman-1959/.

DOI: 10.1021/acs.inorgchem.6b00700
Inorg. Chem. 2016, 55, 9964−9972